Synthesis and Characterization of Metal Sulfates Loaded Palm Empty Fruit Bunch (PEFB) for Biodiesel Production

(Sintesis dan Pencirian Sulfat Logam Dimuatkan Tandan Kosong Kelapa Sawit (PEFB) untuk Pengeluaran Biodiesel)

RAHILA ISHFAQ*, NURUN NAJWA RUSLAN, NURSYAFREENA ATTAN, SUZI SALWAH JIKAN & AMIRA SARYATI AMERUDDIN

ABSTRACT

Biodiesel has been globally accepted as a green substitute for diesel fuel. However, the insecurity of food raised with the application of edible sources in biodiesel production has caused much debate. The feasible alternative technique is the use of inedible and low-grade sources such as palm fatty acid distillate (PFAD). In this work, the production of biodiesel (FAME) from PFAD using solid acid catalysts (SACs) derived from palm empty fruit bunch (PEFB) is investigated. The SACs were synthesized through impregnation of different metal sulfate precursors, i.e. ferrous sulfate heptahydrate $(FeSO_4.7H_2O)$, copper sulfate pentahydrate $(CuSO_4.5H_2O)$, and magnesium sulfate heptahydrate $(MgSO_4.7H_2O)$ over PEFB. SEM-EDX observations found that impregnation and then calcination resulted in attachment of sulfur (S) and improved surface porosity. FT-IR analysis showed that there were distinct interactions between metal sulfates and PEFB. XRD characterization showed that the prepared catalysts have a crystalline structure. Besides, the catalytic activity of the SACs was closely associated with their acid densities measured by the titration method. Fe-PEFB catalyst showed the highest acid density (2.44 mmol/g) among the catalysts studied. To study the effect of process parameters on FFA conversion (%), optimization of methanol: PFAD molar ratio, catalyst dosage, reaction temperature, and reaction time was conducted. Maximum FFA conversion of 89.1% was obtained over Fe-PEFB while Cu-PEFB and Mg-PEFB achieved an FFA conversion of 63 and 56.5%, respectively, under the optimum reaction conditions. Thus, the present study offers a sustainable and environmentally benign method for biodiesel production.

Keywords: Biodiesel; biomass waste; esterification; impregnation; palm fatty acid distillate; solid acid catalysts

ABSTRAK

Biodiesel telah diterima secara global sebagai pengganti hijau untuk bahan api diesel. Walau bagaimanapun, ketidakamanan makanan yang dibangkitkan dengan penggunaan sumber yang boleh dimakan dalam pengeluaran biodiesel telah menyebabkan banyak perdebatan. Teknik alternatif yang boleh dilaksanakan ialah penggunaan sumber yang tidak boleh dimakan dan bermutu rendah seperti sulingan asid lemak kelapa sawit (PFAD). Dalam kerja ini, pengeluaran biodiesel (FAME) daripada PFAD menggunakan mangkin asid pepejal (SAC) yang diperoleh daripada tandan kosong kelapa sawit (PEFB) telah dikaji. SAC telah disintesis melalui penjejalan pelopor sulfat logam yang berbeza, iaitu, ferus sulfat heptahidrat $(FeSO_4.7H_2O)$, kuprum sulfat pentahidrat $(CuSO_4.5H_2O)$ dan magnesium sulfat heptahidrat $(MgSO_4.7H_2O)$ berbanding PEFB. Pemerhatian SEM-EDX mendapati bahawa penjejalan dan kemudian pengkalsinan menghasilkan perlekatan sulfur (S) dan liang permukaan bertambah baik. Analisis FT-IR menunjukkan bahawa terdapat interaksi yang berbeza antara sulfat logam dan PEFB. Pencirian XRD menunjukkan bahawa pemangkin yang disediakan mempunyai struktur hablur. Selain itu, aktiviti pemangkin SAC berkaitan dengan ketumpatan asid mereka yang diukur dengan kaedah pentitratan. Mangkin Fe-PEFB menunjukkan ketumpatan asid tertinggi (2.44 mmol/g) antara mangkin yang telah dikaji. Untuk mengkaji kesan parameter proses terhadap penukaran FFA (%), pengoptimuman metanol:nisbah molar PFAD, dos mangkin, suhu tindak balas dan masa tindak balas telah dijalankan. Penukaran FFA maksimum sebanyak 89.1% diperoleh berbanding Fe-PEFB manakala Cu-PEFB dan Mg-PEFB mencapai penukaran FFA sebanyak 63 dan 56.5%, dalam keadaan tindak balas yang optimum. Oleh itu, kajian ini menawarkan kaedah yang mampan dan jinak alam sekitar untuk pengeluaran biodiesel.

Kata kunci: Biodiesel; mangkin asid pepejal; pengesteran; penjejalan; penyulingan asid lemak sawit; sisa biojisim

Introduction

Diminishing energy resources and the distress over global warming led to the development of biodiesel. It is green, energy-efficient, non-toxic, biodegradable, and renewable sources of energy. Moreover, the sulfur contents in biodiesel are lower and have no carcinogens (Sharma et al. 2008; Suppalakpanya et al. 2010). Biodiesel can be defined as a blend of monoalkyl esters obtained from vegetable oils or animal fats through esterification-transesterification reaction with an alcohol by applying acidic or basic catalysts (Watanabe et al. 2000).

Typically, biodiesel is obtained from various plant oils like soybean oil (Jacobson et al. 2008; Rezaei et al. 2013; Supamathanon et al. 2011; Uzun et al. 2012; Yu et al. 2010), palm oil (Marinković et al. 2016), coconut and cotton oil (Marinković et al. 2016), colza oil (Sirisomboonchai et al. 2015; Soriano Jr. et al. 2009), sesame oil (Nautiyal et al. 2014) sunflower and mustard oils (Nakatani et al. 2009). However, dependence on edibles as feedstock for biodiesel production has created severe issues, like the 'food versus fuel' disputation due to generation of biodiesel from human nutriments and the exhaustion of farmland and water reservoirs (Chai et al. 2014). Moreover, the hefty price of the feedstock (edible vegetable oil), which is 60 - 95% of the entire expenditure of biodiesel generation, makes this source of energy less competitive in the fuel industry (Chai et al. 2014; Hayyan et al. 2010). Thus, choosing the right feedstock to obtain biodiesel can overcome this problem significantly.

One of the potential substitute feedstocks for biodiesel generation, mainly in the exhaustive palm oil-producing areas, is PFAD. A considerable amount (over 700,000 metric tons) of PFAD has been generated in Malaysia as a side product from the refinery procedure in palm oil industries (Ping & Yusof 2009). It is a pale-yellow solid which is composed of 80% free fatty acid (FFA). This FFA mainly comprises palmitic acid, oleic acid, linoleic acid, myristic acid, stearic acid, and a fraction of squalene (Lokman et al. 2014). However, using such feedstock in base-catalyzed transesterification is not recommended as it has higher FFAs content, which results in saponification.

In the traditional esterification process, sulfuric acid (H_2SO_4) is generally used as a homogeneous acid catalyst. The utilization of homogeneous acid catalysts leads to many disadvantages such as corrosion of instruments, difficult catalyst recovery, and production of acidic water in the purification process, which is a significant issue on the industrial level (Dong et al. 2015).

In order to eliminate these disadvantages, various types of SACs such as ferric alginate (Peng-Lim et al. 2012), sulfonated carbon nanotubes (Shuit & Tan 2014), resin (Chang et al. 2013), and polymer (Xia et al. 2012) have been investigated. However, the high-cost materials and preparation methods decreased their commercial applications. Hence, the development of SACs from inexpensive biomass waste to form biodiesel from low-grade feedstock could be a potential and high interest. 10% out of 85.5% of the total palm biomass is used to produce oil. Thus, Malaysia has an abundant source of palm biomass that could be used for the synthesis of catalysts as raw material and as a feedstock for biodiesel generation.

Thushari and Babel (2018b) reported 91% biodiesel yield in 14 h reaction time when palm empty fruit bunch (PEFB) derived SAC was used for biodiesel generation from waste palm oil through esterification.

Ezzah-Mahmudah et al. (2016) investigated the preparation of SAC from *Anadara granosa* through the impregnation-calcination method. The catalyst was prepared by doping of iron (III) oxide (Fe_2O_3) on CaO and then calcined at 500 °C. The obtained catalyst (Fe_2O_3/CaO) was employed to generate biodiesel by a single step process. Over 90% conversion was achieved under the optimized reaction conditions. Moreover, cadmium sulfate templated on glycine heterogeneous catalyst has been reported by Paul (2018). From the characterization study, it was found that the catalyst has a crystalline structure with two-dimensional layers due to the alternate connection of cadmium and sulfate.

To the best of our knowledge, no research study on the catalytic activity of different metal sulfates impregnated PEFB SACs has been published yet, to generate biodiesel from PFAD. In this study, the main objective was to prepare PEFB based SACs for biodiesel generation using noncorrosive chemicals and environmentally friendly preparation methods. A comprehensive physicochemical characterization that is by Fourier Transform Infra-Red (FT-IR) spectroscopy, Scanning Electron Microscopy-Energy Dispersive X-ray spectroscopy (SEM-EDX), and X-Ray Diffraction (XRD) analyses were performed for the prepared SACs. Acid densities of the SACs were calculated by the titration method. The influence of significant process variables, such as methanol: PFAD mole ratio, catalyst amount, reaction temperature, and reaction time on FFA conversion (%) were also studied.

EXPERIMENTAL DETAILS
MATERIALS AND REAGENTS

Palm empty fruit bunch (PEFB) and palm fatty acid distillate (PFAD) were collected from Felda Palm Industries Sdn Berhad and Keck Seng(M) Berhad, Malaysia, respectively. Methanol (CH_3OH) (99.99%), sodium hydroxide (NaOH) (99%), citric acid ($C_6H_8O_7$) (99.9%), copper sulfate pentahydrate ($CuSO_4.5H_2O$) ($\geq$99%) were purchased from Emery Oleochemicals Malaysia. Ferrous sulfate heptahydrate ($FeSO_4.7H_2O$) ($\geq$99%), magnesium sulfate heptahydrate ($MgSO_4.7H_2O$) ($\geq$99%), and 2-propanol (C_3H_8O) were obtained from Sigma-Aldrich. Potassium hydroxide (KOH) (99%) and sodium chloride (NaCl) (99%) were purchased from Vchem. All the chemicals were analytical grades.

SYNTHESIS OF SACS

SACs were synthesized by the impregnation-calcination method. The collected shredded PEFB was first chopped manually into small pieces (25 mm) and dried in a drying oven for 48 h. The dried sample was ground to powder using a grinder (Philips HR2056) and was sieved through a 120-mesh sieve to get 120-125 µm particle size. The powder was washed repeatedly using deionized water for the removal of dust and other impurities such as calcium (Ca), potassium (K), aluminum (Al), and silicon (Si), which are attached on the surface of the raw PEFB and later dried for 24 h. The dried sample was treated with NaOH (0.5 M) for 1 h at ambient temperature and afterward washed to clean it from the excessive NaOH. After drying, the sample was treated with citric acid (0.6) to impart acidic properties and to remove any remaining impurities. The acidic sample was washed with hot deionized water repeatedly and then dried in a drying oven at 140 °C for 12 h. This method was modified from Sajab et al. (2011). The obtained clean PEFB precursor was divided into 3 parts and impregnated with metal sulfates ($FeSO_4.7H_2O$, $CuSO_4.5H_2O$, and $MgSO_4.7H_2O$) at concentrations of 20% w/v. This process was carried out at room temperature for 2 h. After that, the impregnated samples were filtered and dried at 110 °C for 24 h, followed by calcination at 500 °C for 3 h. The obtained SACs were named Fe-PEFB, Cu-PEFB, and Mg-PEFB, based on the impregnated metal sulfate.

CHARACTERIZATION OF SACS

Morphological and elemental compositions of the catalysts were examined by SEM-EDX (Hitachi VP-SEM SU1510) where the porosity of the catalysts was determined using ImageJ software and specific surface area of the catalysts was calculated using (1).

$$Specific\ Surface\ Area = \frac{6 \times 10^3}{\tau \times \rho} \qquad (1)$$

where τ is the crystallite size of the catalyst, and ρ is the density of the material (sample) (Theivasanthi & Alagar 2010).

For functional groups investigation of the catalysts, raw and pre-treated samples, FT-IR spectrometer (PerkinElmer spectrum 100 FT-IR spectrometer) was deployed. Crystallographic properties analysis of the prepared catalysts was performed by XRD (XRD Bruker D8 Advance). XRD patterns were recorded under the following conditions: WL = 1.540600, steptime = 15.400000, stepsize = 0.019730, tube-voltage = 40 kV and tube-current = 40 mA. The total acid density of –SO_3H groups on the surface of the prepared catalysts was determined by the titration method using 0.1 N NaOH and 1 N NaCl solution as given in the literature (Lee 2013; Xue et al. 2016). Acid densities of the catalysts were calculated by using (2).

$$Acidity\ of\ catalyst = V \times \frac{N}{W} \qquad (2)$$

where V represents the volume; N represents the normality; and W represents the weight of the catalyst.

ESTERIFICATION OF PFAD TO BIODIESEL

The catalytic activities of the synthesized SACs were evaluated through the esterification of PFAD to biodiesel. The effect of the process parameters was investigated using the monothetic analysis, also known as one-variable-at-a-time (OVAT) approach (Alsultan et al. 2017). Typically, esterification reaction was performed by changing one parameter at a time while maintaining the other parameters constant. This is the simplest method to select the significant parameters that affect the biodiesel yield (Abdulkareem-Alsultan et al. 2019). The conventional reflux method was used for the esterification of PFAD. About 20 g of PFAD, different dosages of the synthesized SACs (3 - 7 wt%), and methanol : PFAD mole ratios (10:1 - 14:1) were mixed in 250 mL 2-necked round bottom flask followed by heating at (50 - 70 °C) for (2-6 h) reaction times at constant stirring rate (300 rpm). After the reaction was completed, the SAC was removed from the product through filtration. The product was transferred into a separator funnel and kept undisturbed for 12 h to achieve

complete phase separation. In the separator funnel, products (biodiesel) constitute the bottom layer, while the top layer consists of a blend of water and methanol. The product was heated at 70 °C to eliminate the moisture and to evaporate excessive methanol.

FAME CONVERSION

The FAME yield was calculated as FFA conversion (%) based on the difference of the acid value of the feedstock (PFAD) and product (FAME) using AOCS 5 a-40 standard method (Lathiya et al. 2018). The acid value of PFAD and the product was determined using (3).

$$Acid\ value \left(mg \frac{KOH}{g} \right) = \frac{((V_f - V_i) \times N \times 56.1}{W} \times 100\% \quad (3)$$

where V_f is the final volume of standard KOH used in titration (mL); V_i is the initial volume of standard KOH used in titration (mL); N is the normality of standard KOH; and W is the mass of sample (g).

Equation 4 was used for calculating FFA conversion (%).

$$Reaction\ Conversion\ (\%) = \frac{AV_f - AV_p}{AV_f} \times 100\% \quad (4)$$

where AV_f is the acid value of feedstock while AV_p is the product's acid value.

RESULTS AND DISCUSSION

CHARACTERIZATION OF CATALYSTS
CRYSTALLOGRAPHIC ANALYSIS

XRD pattern of the Fe-PEFB (Figure 1(a)) is well defined and matches the hexagonal structure of ferric oxide (Fe_2O_3) (ICDD, card no: 033-0664). The peaks at $2\theta = 24.26°$, $33.35°$, $35.72°$, $40.93°$, $49.53°$, $54.13°$, $57.67°$, $62.51°$, $64.07°$, and $75.59°$ can be index to (012), (104), (110), (113), (024), (116), (018), (214), (300), and (220) lattice planes of hexagonal iron oxide (Fe_2O_3), respectively (ICDD card no: 00-033-0664). Average crystallite size of Fe-PEFB, estimated by the Debye Scherrer equation, is 37.458 nm. The Fe or Fe_2O_3, which is formed due to decomposition and oxidation of ferrous sulfate during calcination, is also known as a good promoter for the reactions which involve feedstock with high FFA content (Mengyu et al. 2009). The diffraction pattern and crystalline phase of Fe_2O_3 agree well with the results of Zhu et al. (2015).
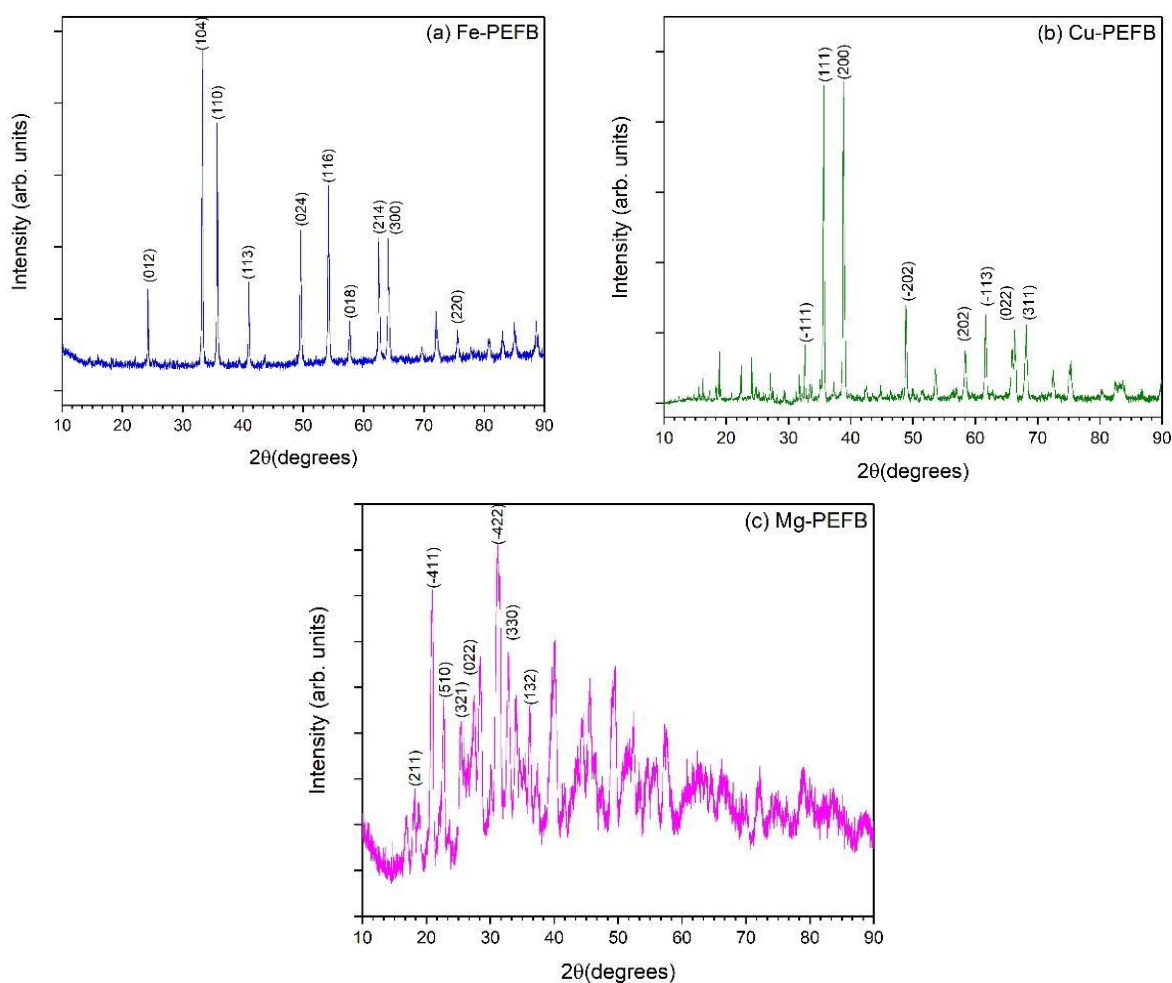

FIGURE 1. XRD patterns of (a) Fe-PEFB, (b) Cu-PEFB, and (c) Mg-PEFB

Figure 1(b) shows the XRD pattern of Cu-PEFB. All the diffraction peaks are well defined, showing the crystalline structure of Cu-PEFB and indicate the formation of CuO with monoclinic structure. The peaks appeared at 2θ = 32.63°, 35.65°, 38.79°, 48.84°, 58.39°, 61.62°, 65.90°, and 68.16° were assigned to the corresponding (-111), (111), (200), (-202), (202), (-113), (022), and (311) planes, respectively (ICDD card no: 01-080-1916). The average crystallite size of the Cu-PEFB was calculated to be 47.76 nm using the Debye Scherrer equation. All the diffraction peaks in the Cu-PEFB pattern indicate the formation of copper oxide (CuO), as reported by Arun et al. (2015), Ekmekyapar et al. (2015), and Sundar et al. (2018).

XRD pattern of Mg-PEFB is shown in Figure 1(c). The peaks seem to be less crystallized than Fe-PEFB and Cu-PEFB. The peaks appeared at 2θ = 18.05°, 20.73°, 22.75°, 25.30°, 27.55°, 32.83°, 33.99°, and 36.18° and they were assigned to the corresponding (211), (-411), (510), (321), (022), (-422), (330), and (132) lattice planes of hexagonal magnesium sulfite hexahydrate. (ICDD card no: 00-024-0721). The average crystallite size of Mg-PEFB estimated by Debye Scherrer equation is 14.95 nm.

High crystallinity is associated with high porosity and larger surface area. The conversion of poorly crystalline CPPs evaluated the influence of crystallinity on surface area and porosity into well crystalline CPPs with a remarkable increase in surface area and pore volume (Ji et al. 2018).

MORPHOLOGICAL AND ELEMENTAL ANALYSIS

Figure 2(a) shows the external surface of the raw PEFB and pre-treated PEFB (treated with NaOH and citric acid). Many pores are visible on the surface of pre-treated PEFB Figure 2(b). This is due to the removal of adhered impurities such as potassium (K), aluminum (Al), silicon (Si), and dust particles during the washing and pre-treatment process (Gowri Krishnan et al. 2016).
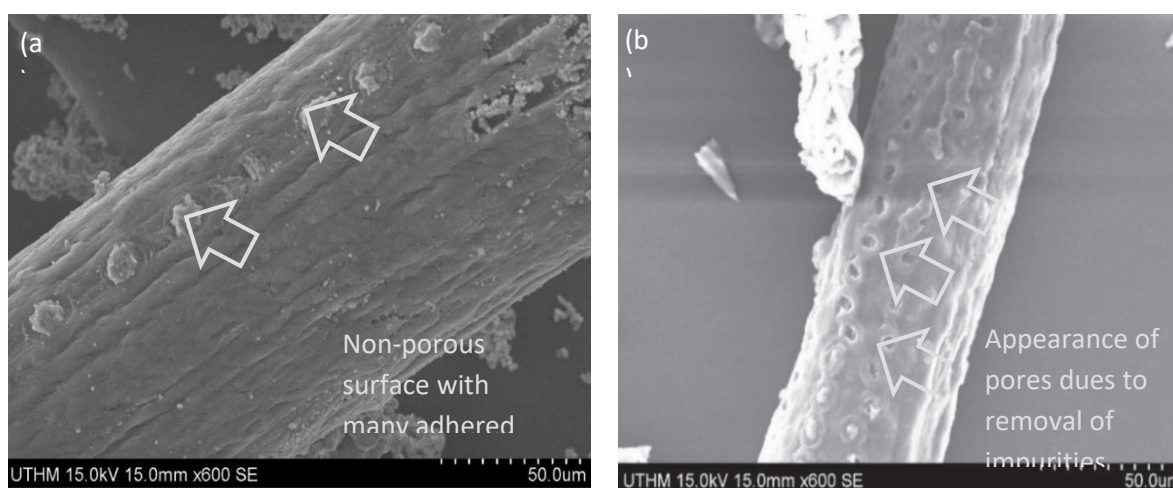

FIGURE 2. SEM images of (a) Raw PEFB and (b) Pre-treated PEFB

Figure 3(a), 3(b) and 3(c) shows the transverse morphology of SACs impregnated with $FeSO_4.7H_2O$, $CuSO_4.5H_2O$, and $MgSO_4.7H_2O$, respectively. Figure 3(a) and 3(b) demonstrates that the surface of Fe-PEFB and Cu-PEFB consist of a significant number of particle agglomerates, and pores with various sizes and shapes. Similar morphology was reported by Lathiya et al. (2018) and Liu et al. (2018). The formation of the agglomerated porous structure is due to the impregnation and calcination process. During calcination, metal sulfates undergo decomposition and get converted into their respective oxides. Cracking, partial destruction of the structure and formation of new compounds may also occur, primarily if the calcination is carried out at higher temperatures. Furthermore, amorphous material can become crystalline, along with variations in the pore structure (Knözinger & Kochloefl 2000). However, no such agglomerates and pores were found in PEFB impregnated with $MgSO_4.7H_2O$ but a bulky and less porous surface was observed, as shown in Figure 3(c). This can be attributed to partial decomposition, and poor interaction of $MgSO_4.7H_2O$ with PEFB as XRD analysis

shows the formation of magnesium sulfite hexahydrate, unlike $FeSO_4.7H_2O$ and $CuSO_4.5H_2O$, which are entirely decomposed. The results of the porosity of the catalysts is given in Table 1. Figure 3(a), 3(b), and 3(c) are used for porosity calculation.

TABLE 1. Porosity of catalysts calculated using imageJ software

Catalyst	Porosity percentage
Fe-PEFB	6.46%
Cu-PEFB	4.98%
Mg-PEFB	4.07%

TABLE 2. Surface area of catalysts calculated using (1)

Catalyst	Surface area
Fe-PEFB	30.568 m²/g
Cu-PEFB	19.909 m²/g
Mg-PEFB	150.87 m²/g

The surface areas of the three catalysts is listed in Table 2. Although Mg-PEFB has larger surface area, it has lower porosity and low acid density than the other two catalysts.
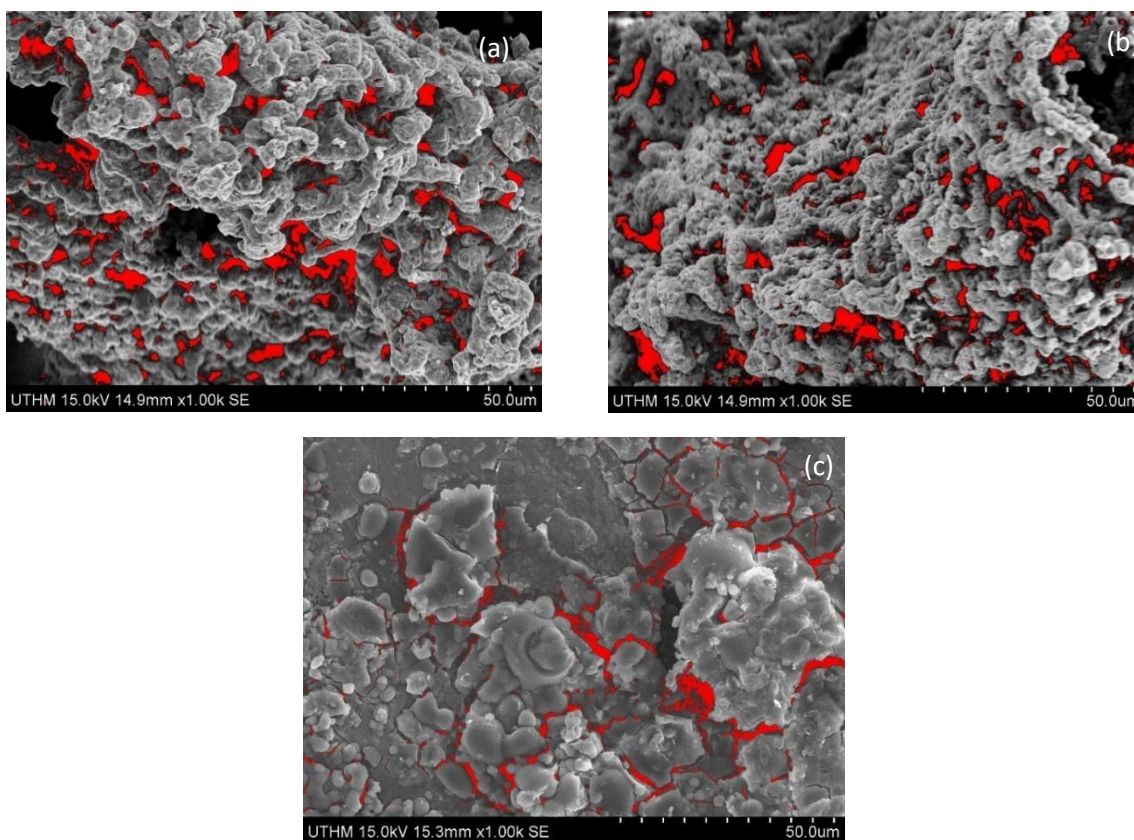

FIGURE 3. SEM images of (a) Fe-PEFB, (b) Cu-PEFB and (c) Mg-PEFB where the red color indicates pores

The successful impregnation of metal sulfates over PEFB is reconfirmed by the qualitative elemental analysis using EDX. The elemental composition of the raw PEFB, pretreated PEFB, and synthesized SACs are shown in Table 3. The presence of K, Al, and Si as impurities is shown by EDX in raw PEFB. However, these elements were not found in pre-treated PEFB and the catalysts. It shows that the pre-treatment process successfully removed impurities.

Moreover, it was observed that the S content of the catalysts has increased while carbon (C) and O content have decreased as compared to the raw PEFB and pre-treated PEFB. These variations are because of sulfonation, dehydration, and deoxygenation of the PEFB during impregnation and calcination (Malins et al. 2016). According to EDX analysis, Cu-PEFB has the highest weight percentage of S (7.38%), followed by Mg-PEFB (7.26%) and Fe-PEFB (6.41%). The presence of S in PEFB derived SAC confirms the impregnation of metal sulfate on the surface of catalysts and enables them to be treated as SACs.

TABLE 3. Elemental composition of raw PEFB, pre-treated PEFB, and SACs in wt% (C=Carbon, O=Oxygen, S=Sulphur, Fe=Iron, Cu=Copper, Mg=Magnesium, Al=Aluminium, Si=Silicon, K=Potassium)

| Sample | C | O | S | Fe | Cu | Mg | Impurities | | |
							Al	Si	K
Raw	58.11	40.93	ND*	ND	ND	ND	0.44	0.18	0.34
Pre-Treated	50.54	49.46	ND	ND	ND	ND	ND	ND	ND
Fe-PEFB	ND	42.41	6.41	51.19	ND	ND	ND	ND	ND
Cu-PEFB	ND	36.94	7.38	ND	55.68	ND	ND	ND	ND
Mg-PEFB	34.69	48.28	7.26	ND	ND	9.77	ND	ND	ND

[a]Not detected

FUNCTIONAL GROUP ANALYSIS

The FT-IR spectra of raw PEFB, pre-treated PEFB, and synthesized SACs are shown in Figure 4. As compared to raw and pre-treated PEFB, new bands can be observed with a frequency of 986.59 cm^{-1} and 958.77 cm^{-1} in Fe-PEFB and Cu-PEFB catalysts, respectively. These bands are attributed to sulfate ions (Ariza et al. 2002). Furthermore, the band at 1110.55 in Fe-PEFB represents asymmetric stretching vibrations of sulfur dioxide (SO_2) and $-SO_3H$ group. The high efficiency of Fe-PEFB is due to the presence of these groups. However, no sulfur (S) band appeared in the Mg-PEFB catalyst, which indicates the absence of $-SO_3H$ group. The acid densities of SACs are mainly attributed to $-SO_3H$ group, which is covalently bonded to the polyaromatic carbon structure of SAC (Lokman et al. 2015). The stretching bands at 1622.69, 1623.15, and 1646.43 cm^{-1} are the characteristic peaks of typical carbonyl functional groups (C=O) in all the three synthesized catalysts (Flores et al. 2019; Okamura et al. 2006). The bands appeared at 3036.94 - 3343.55 cm^{-1} in raw PEFB, pre-treated PEFB, and the catalysts are assigned to phenolic and alcoholic hydroxyl (OH) groups (Thushari & Babel 2018a). Present results verify the presence of $-SO_3H$, $-COOH$, and $-OH$ groups on the surface of the synthesized SACs. The SACs showed FT-IR bands with different positions and intensities. This is due to the different interactions between metal sulfates and the surface of PEFB. Different interaction of metal sulfates is due to their different degree of surface acidity and electronegativity of the metal ion.

ACID DENSITY

The efficiency of the SAC is generally referred to the existed $-SO_3H$ groups, its number, strength, and location on the surface of SAC. However, the overall acid density of the SAC is primarily because of $-SO_3H$, $-COOH$ and $-OH$ groups. Among these three groups $-SO_3H$ groups add significantly in esterification and transesterification reactions (Su & Guo 2014; Thushari & Babel 2018a; Zong et al. 2007). The highest acid density (2.44 mmol/g) was exhibited by the Fe-PEFB catalyst, followed by Cu-PEFB (0.96 mmol/g) and Mg-PEFB (0.78 mmol/g). These values
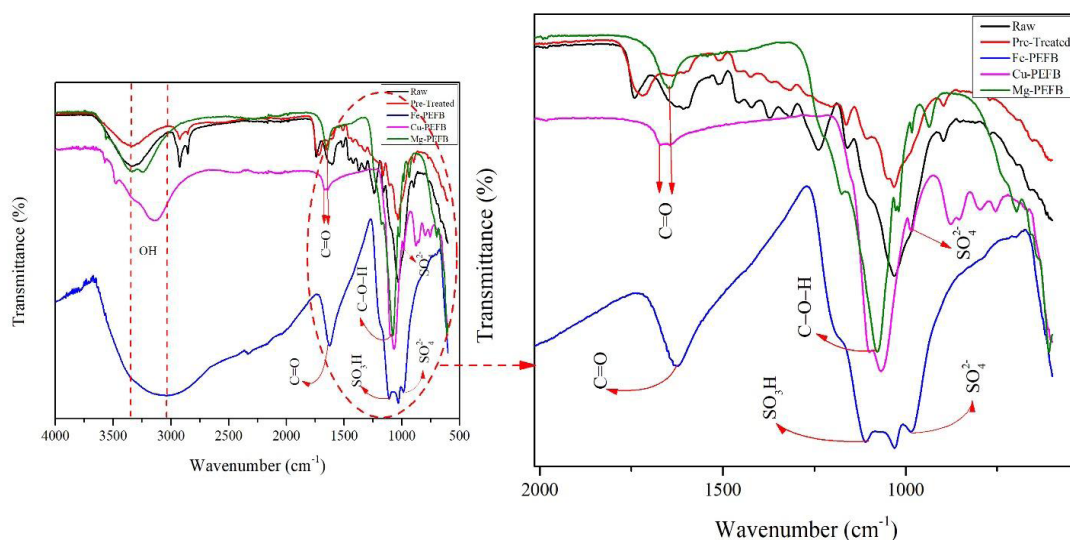
FIGURE 4. FT-IR spectra of Fe-PEFB, Cu-PEFB, and Mg-PEFB

explain the high catalytic performance of the Fe-PEFB catalyst, followed by Cu-PEFB and Mg-PEFB. The high acid density of Fe-PEFB catalyst may be due to the greater interaction of $Fe_2SO_4.7H_2O$ with PEFB because of its high electronegativity and high acid strength than $CuSO_4.5H_2O$ and $MgSO_4.7H_2O$. The highly porous surface of Fe-PEFB, as shown in Figure 3(b), also contributes to high acidity by holding more –SO_3H groups, which are also confirmed by FT-IR results. The catalytic activity of Mg-PEFB is due to the presence of weak –COOH and –OH groups, as shown in the FT-IR spectrum (Figure 4).

COMPOSITION OF CRUDE PFAD

The acid value of the crude PFAD was determined to be 258.06 mg KOH/g as calculated by AOCS (American oil chemist's society) method. This is beyond the value recommended for traditional alkali catalyzed biodiesel synthesis (Su & Guo 2014). The fatty acid (FA) composition of the PFAD was studied by the Gas Chromatography-Flame ionization detector (GC-FID). Composition of PFAD varies and depends upon quality of crude palm oil and on the processed conditions at which it was refined. In one reported study, PFAD was found to be 96.1 % of FFAs and glycerides (Gapoor et al. 2002). Chang et al. (2016) reported FFA content in the range of 65.70 - 94.68 % in the collected PFAD samples. However, Palmitic acid and oleic acid were the dominant fatty acids in the majority of the studies (Akinfalabi et al. 2019; Chang et al. 2016; Ping & Yusof 2009) including the current study. The FA components percentage of the PFAD was found to be comparable to previous reported values and is shown in Table 4.

TABLE 4. Fatty acid composition of PFAD

Fatty acid	Percentage
Palmitic Acid	49.5%
Oleic Acid	30.0%
Linoleic Acid	6.0%
Stearic Acid	2.5%
Triglycerides (TG)	9%
Diglycerides (DG)	2%
Monoglycerides (MG)	1%

CATALYTIC ACTIVITY OF THE SACS

The catalytic activity of SACs is frequently attributed to the presence of $-SO_3H$ groups. However, the actual activity is best determined through their performance when used for their intended application. In the present study, catalytic activities (FFA conversion (%)) of the prepared SACs were evaluated through the esterification of PFAD to biodiesel and were compared under the same reaction conditions. The results are given in Table 5.

FFA conversion after esterification varied significantly among the prepared SACs tested. Table 5 shows FFA conversion (%) under optimum reaction conditions, using the prepared SACs and FFA conversion without the catalyst. The order of catalytic activity in terms of FFA conversion (%) among the synthesized SACs was Fe-PEFB (89.1%) > Cu-PEFB (63%) > Mg-PEFB (56.5%). The catalytic activities of the SACs are well agreed with their acid densities that are measured by the titration method. The high catalytic activity of Fe-PEFB is attributed to the synergistic effect of the $-SO_3H$ and the presence of Fe_2O_3. Fe_2O_3 that is formed due to the decomposition of $Fe_2SO_4.7H_2O$ during calcination (as confirmed by XRD analysis) does not contribute to catalytic activity directly. However, due to the high surface area of these small particles, reactants could be easily adsorbed and hence make them readily available to the surrounding acid functional groups (D'Souza et al. 2018).

TABLE 5. Comparison of the catalytic activities of the synthesized SACs in the esterification of PFAD

Catalyst	Catalyst dosage	Methanol: PFAD ratio	Reaction Temp	FFA conversion (%)	
				after 4 h	after 6 h
Fe-PEFB	5wt%	14:1	70 °C	84.8%	89.1%
Cu-PEFB	5wt%	14:1	70 °C	63 %	60.9%
Mg-PEFB	5wt%	14:1	70 °C	56.5%	52.2%

In Cu-PEFB, stretching bands of sulfate ions along with $-COOH$ and $-OH$ bands were found. Moreover, the low catalytic activity of Mg-B is because of the absence of sulfonic groups, which is confirmed by FT-IR results. This can be attributed to the low decomposition of $MgSO_4.7H_2O$ as confirmed by XRD analysis when compared to $FeSO_4.7H_2O$ and $CuSO_4.5H_2O$ that are entirely decomposed into their respective oxide products.

It can be concluded that the overall activity of the SACs is due to an interconnected system of large pores, hydrophobic surface, and moderate to high concentration of strong acid sites (Lotero et al. 2005). Furthermore, the crystalline structure of Fe-PEFB and Cu-PEFB also contributes towards high catalytic activity since well crystalline structures exhibit larger surface area and high pore volume as compared to poorly crystalline structures (Ji et al. 2018).
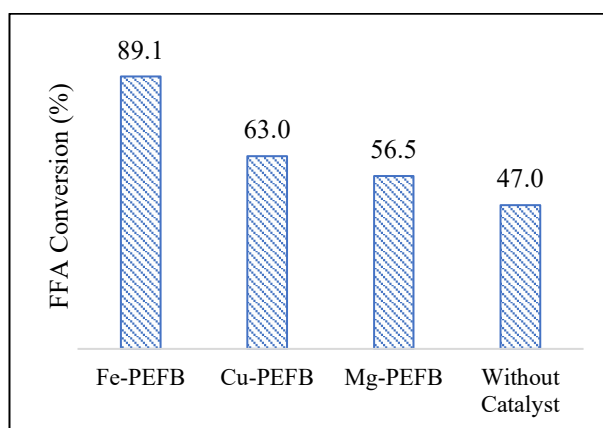

FIGURE 5. Comparison of FFA Conversion (%) achieved with and without catalysts

The different catalytic activity of the SACs can also be attributed to their different interaction with the PEFB surface. The factors that affect the interaction of metal sulfates with the support include surface acidity of the metal sulfate and electronegativity of the central metal ion (Takeshita et al. 1974). Based on these observations, Fe is the most electronegative, has more significant interaction, and maximum selectivity than Cu and Mg. Therefore, Fe-PEFB recorded better catalytic activity as compared to Cu-PEFB and Mg-PEFB. The FFA conversion without catalyst is due to the high temperature (70 °C) which reduces the strength of the intermolecular hydrogen bonds that exist between the alcohol molecules, leading to a significant reduction in the alcohol dielectric constant (Hoffmann & Conradi 1998). Polarity reductions due to the weakening of the hydrogen bonds enhance nucleophilic attack on the carbonyl carbon by the alcohol, thus resulting in FFA conversion (Hoffmann & Conradi 1998).

OPTIMIZATION OF THE PROCESS PARAMETERS
EFFECT OF METHANOL : PFAD MOLE RATIO ON FFA CONVERSION

A critical parameter that ensures completion of the reaction and high FFA conversion is the quantity of alcohol used. In the present study, methanol was used in 3 different molar ratios (10:1, 12:1, 14:1), as shown in Figure 6(a). During methanol: PFAD mole ratio optimization, the other three parameters were kept constant, which are the catalyst dosage (3wt%), the reaction temperature (70 °C), and contact hours (4 h). It is clear from Figure 6(a) that by increasing methanol: PFAD mole ratio, FFA conversion (%) also increases. Since esterification is a reversible process; therefore, an excessive quantity of methanol is needed to push the reaction to the right (forward direction). However, a further increase in the amount of methanol drives the process to the left (backward direction). This is because of the excess water formation during esterification and thus pushes the reaction in the reverse direction by reacting with the feedstock (Akinfalabi et al. 2017). At 14:1 methanol: PFAD, the maximum FFA conversion (%) of 82.6% was obtained when Fe-PEFB was applied. Over Cu-PEFB and Mg-PEFB, the highest conversion (%) under these reaction conditions was 58.7 and 52.2%, respectively. As a result, 14:1 methanol: PFAD mole ratio was selected as an optimum ratio for further work. Zhang and Jiang (2008) optimized 24:1 methanol: oil mole ratio whereas Flores et al. (2019) utilized 20:1 methanol: oil mole ratio in the esterification of oleic acid. It clearly shows that as compared to other related research studies, modest methanol: PFAD mole ratio was used in the present study.

EFFECT OF CATALYST DOSAGE ON FFA CONVERSION

Figure 6(b) shows three different SACs dosages (3, 5, and 7 wt%) used for FFA conversion in PFAD. When the amount of catalyst was increased from 3 to 7 wt%, keeping the other parameters constant, FFA conversion was increased from 82.6 to 86.9% over Fe-PEFB. The initial conversion of 82.6% over Fe-PEFB, 58.7% over Cu-PEFB, and 52.2% over Mg-PEFB when 3 wt% catalyst was used, showed 3, 5, and 4% increase in FFA conversion, respectively, when 7 wt% catalyst was added. As a result of this, 7 wt% catalyst dosage of Fe-PEFB was optimized. However, over Cu-PEFB and Mg-PEFB similar FFA conversion was observed at 5 and 7 wt%. Hence, 5 wt% was chosen as an optimum catalyst dosage of Cu-PEFB and Mg-PEFB for further work.

From these results, it is concluded that though an adequate amount of catalyst is required for high conversion, excess of catalyst did not increase the FFA conversion. This was due to quite enough interaction of the catalyst with the methanol, while the PFAD had already reached the point of equilibrium (Yujaroen et al. 2009). Guo et al. (2012) also optimized 7 wt% catalyst dosage to achieve high FFA conversion. Whereas Flores et al. (2019) and González et al. (2017) used an excess of 10 wt% of the prepared catalyst and obtained up to 96% FFA conversion.

EFFECT OF REACTION TEMPERATURE ON FFA CONVERSION

The influence of reaction temperature on FFA conversion was investigated by performing esterification at three distinct temperatures that are 50, 60 and 70 °C; while the other three parameters were maintained constant throughout the reactions. As expected, an increase in temperature resulted in increased FFA conversion by increasing the rate of esterification. As illustrated in Figure 6(c), FFA conversion was very low at 50 °C that is 73.9% over Fe-PEFB, 49.8% over Cu-PEFB, and 50% over Mg-PEFB. At 70 °C, 86.9% FFA conversion was recorded over Fe-PEFB. 63 and 56.5% FFA conversions were observed over Cu-PEFB and Mg-PEFB, respectively. Excessive methanol vapors are produced at a higher temperature, which effectively combines with the feedstock and results in high conversion (Encinar et al. 2012). This may be the reason for high conversion at 70 °C over each catalyst. Hence, 70 °C was optimized

for further study. A similar study was conducted by Thushari and Babel (2018a) and González et al. (2017). They achieved high FFA conversion at 70 and 140 °C, respectively.

EFFECT OF REACTION TIME ON FFA CONVERSION

The effect of reaction time was investigated under the optimized methanol: PFAD mole ratio, catalyst dosage, and reaction temperature. FFA conversion was observed at various reaction times from 2-6 h. Results presented in Figure 6(d) shows that enough contact time was required to obtain maximum FFA conversion. Greater

FFA conversion (%) was obtained with an increase in reaction time (2-6 h) over the Fe-PEFB catalyst that is from 71.7 to 89.1%. However, over Cu-PEFB and Mg-PEFB, FFA conversion increased until 4 h, that is from 58.7 to 63% and 54.3 to 56.5%, respectively, and then started decreasing. The highest conversion over both Cu-PEFB and Mg-PEFB was observed after 4 h of reaction time. Hence, the reaction time of 6 h was optimized for Fe-PEFB and 4 h for Cu-PEFB and Mg-PEFB catalyzed esterification. Dehkhoda et al. (2010) optimized 3 h of reaction time to obtain optimum biodiesel production. Similarly, Lathiya et al. (2018) achieved high conversion after 4.5 h.
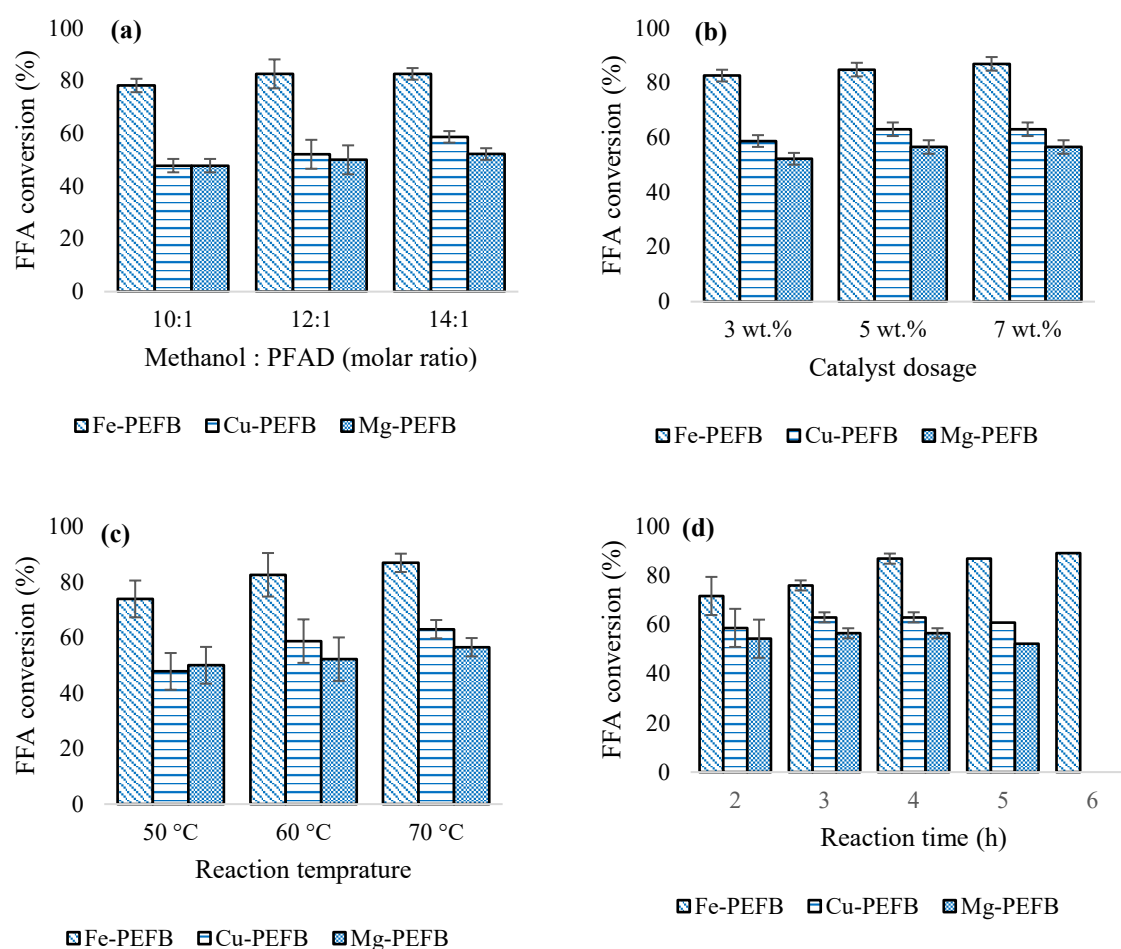

FIGURE 6. Optimization of the process parameters; (a) Effect of methanol : PFAD mole ratio (10:1, 12:1, 14:1) on FFA conversion (%) (catalyst dosage 3 wt%, 4 h reaction time at 70 °C), (b) Effect of catalyst dosage (3, 5, 7 wt%) on FFA conversion (%) (methanol: PFAD mole ratio14:1, 4 h reaction time at 70 °C), (c) Effect of reaction temperature (50, 60, and 70 °C) on FFA conversion (%) (methanol: PFAD mole ration14:1, catalyst dosage 7 wt% Fe-PEFB and 5 wt% Cu and Mg-PEFB, 4 h reaction time), and (d) Effect of reaction time (2 - 6 h) on FFA conversion (%) (methanol: PFAD mole ratio14:1, catalyst dosage 7 wt% of Fe-PEFB and 5 wt% of Cu and Mg-PEFB at 70 °C)

CONCLUSION

In the present work, PEFB obtained SACs were effectively synthesized and applied to form biodiesel from PFAD. A maximum FFA conversion (%) of 89.1% was achieved over Fe-PEFB using 14:1 methanol: PFAD mole ratio, 7 wt% catalyst dosage at 70 °C after 6 h reaction time. High sulfonic acid density of Fe-PEFB profoundly affected the FFA conversion (%). In this work, the reaction temperature was the most significant process parameter after methanol to PFAD molar ratio and reaction time. High FFA conversions were obtained by increasing methanol to PFAD molar ratio and reaction temperature. This study contributed towards the green and economical synthesis of SACs by using nontoxic chemicals and mild preparation conditions rather than the traditional long sulfonation method for SACs catalysts synthesis. Based on the results obtained in this study, it is proposed that PEFB derived SACs are potential catalysts for biodiesel generation from the low-grade feedstock. Moreover, both the processes, catalyst preparation, and biodiesel production are economical and energetically feasible, thereby represent a clean and green method for biodiesel production.

REFERENCES

Abdulkareem-Alsultan, G., Asikin-Mijan, N., Mansir, N., Lee, H.V., Zainal, Z., Islam, A. & Taufiq-Yap, Y.H. 2019. Pyrolytic de-oxygenation of waste cooking oil for green diesel production over Ag_2O_3-La_2O_3/AC nano-catalyst. *Journal of Analytical and Applied Pyrolysis* 137: 171-184.

Akinfalabi, S.I., Rashid, U., Shean, T.Y.C., Nehdi, I.A., Sbihi, H.M. & Gewik, M.M. 2019. Esterification of palm fatty acid distillate for biodiesel production catalyzed by synthesized kenaf seed cake-based sulfonated catalyst. *Catalysts* 9(5): 482.

Akinfalabi, S.I., Rashid, U., Yunus, R. & Taufiq-Yap, Y.H. 2017. Synthesis of biodiesel from palm fatty acid distillate using sulfonated palm seed cake catalyst. *Renewable Energy* 111: 611-619.

Alsultan, G.A., Asikin-Mijan, N., Lee, H., Albazzaz, A.S. & Taufiq-Yap, Y. 2017. Deoxygenation of waste cooking to renewable diesel over walnut shell-derived nanorode activated carbon supported CaO-La_2O_3 catalyst. *Energy Conversion and Management* 151: 311-323.

Ariza, M.J., Jones, D.J. & Rozière, J. 2002. Role of post-sulfonation thermal treatment in conducting and thermal properties of sulfuric acid sulfonated poly (benzimidazole) membranes. *Desalination* 147(1-3) 183-189.

Arun, K., Batra, A., Krishna, A., Bhat, K., Aggarwal, M. & Francis, P.J. 2015. Surfactant free hydrothermal synthesis of copper oxide nanoparticles. *American Journal of Materials Science* 5: 36-38.

Chai, M., Tu, Q., Lu, M. & Yang, Y.J. 2014. Esterification pretreatment of free fatty acid in biodiesel production, from laboratory to industry. *Fuel Processing Technology* 125: 106-113.

Chang, A.S., Sherazi, S.T.H., Kandhro, A.A., Mahesar, S.A., Chang, F., Shah, S.N., Laghari, Z.H. & Panhwar, T. 2016. Characterization of palm fatty acid distillate of different oil processing industries of Pakistan. *Journal of Oleo Science* 65(11): 897-901.

Chang, B., Fu, J., Tian, Y. & Dong, X. 2013. Soft-template synthesis of sulfonated mesoporous carbon with high catalytic activity for biodiesel production. *RSC Advances* 3(6): 1987-1994.

D'Souza, R., Vats, T., Chattree, A. & Siril, P.F. 2018. Graphene supported magnetically separable solid acid catalyst for the single step conversion of waste cooking oil to biodiesel. *Renewable Energy* 126: 1064-1073.

Dehkhoda, A.M., West, A.H. & Ellis, N. 2010. Biochar based solid acid catalyst for biodiesel production. *Applied Catalysis A: General* 382(2): 197-204.

Dong, T., Gao, D., Miao, C., Yu, X., Degan, C., Garcia-Pérez, M., Rasco, B., Sablani, S.S. & Chen, S. 2015. Two-step microalgal biodiesel production using acidic catalyst generated from pyrolysis-derived bio-char. *Energy Conversion and Management* 105: 1389-1396.

Ekmekyapar, A., Demirkıran, N., Künkül, A. & Aktaş, E. 2015. Leaching of malachite ore in ammonium sulfate solutions and production of copper oxide. *Brazilian Journal of Chemical Engineering* 32: 155-165.

Encinar, J., González, J., Martínez, G., Sánchez, N. & Pardal, A. 2012. Soybean oil transesterification by the use of a microwave flow system. *Fuel* 95: 386-393.

Ezzah-Mahmudah, S., Lokman, I.M., Saiman, M.I. & Taufiq-Yap, Y.H. 2016. Synthesis and characterization of Fe_2O_3/CaO derived from *Anadara granosa* for methyl ester production. *Energy Conversion and Management* 126: 124-131.

Flores, K.P., Omega, J.L.O., Cabatingan, L.K., Go, A.W., Agapay, R.C. & Ju, Y.H. 2019. Simultaneously carbonized and sulfonated sugarcane bagasse as solid acid catalyst for the esterification of oleic acid with methanol. *Renewable Energy* 130: 510-523.

Gapoor, A., Hassan, W. & Sulong, M. 2002. Phytochemical for nutraceutical from the by product of palm oil refining. *Palm Oil Develop* 36: 13-19.

González, M., Cea, M., Reyes, D., Romero-Hermoso, L., Hidalgo, P., Meier, S., Benito, N. & Navia, R. 2017. Functionalization of biochar derived from lignocellulosic biomass using microwave technology for catalytic application in biodiesel production. *Energy Conversion and Management* 137: 165-173.

Gowri Krishnan, S., Pua, F.L., Palanisamy, K. & Nabihah, S. 2016. Preparation of oil palm EFB derived solid acid catalyst for esterification reaction: Effect of calcination temperature. *Key Engineering Materials* 701: 117-121.

Guo, F., Xiu, Z.L. & Liang, Z.X. 2012. Synthesis of biodiesel from acidified soybean soapstock using a lignin-derived carbonaceous catalyst. *Applied Energy* 98: 47-52.

Hayyan, A., Alam, M.Z., Mirghani, M.E., Kabbashi, N.A., Hakimi, N.I.N.M., Siran, Y.M. & Tahiruddin, S. 2010. Sludge palm oil as a renewable raw material for biodiesel production by two-step processes. *Bioresource Technology* 101(20): 7804-7811.

Hoffmann, M.M. & Conradi, M.S. 1998. Are there hydrogen bonds in supercritical methanol and ethanol? *The Journal of Physical Chemistry B* 102(1) 263-271.

Jacobson, K., Gopinath, R., Meher, L.C. & Dalai, A.K. 2008. Solid acid catalyzed biodiesel production from waste cooking oil. *Applied Catalysis B: Environmental* 85(1-2): 86-91.

Ji, H., Lee, S., Park, J., Kim, T., Choi, S. & Oh, M. 2018. Improvement in crystallinity and porosity of poorly crystalline metal–organic frameworks (MOFs) through their induced growth on a well-crystalline MOF template. *Inorganic Chemistry* 57(15): 9048-9054.

Knözinger, H. & Kochloefl, K. 2000. Heterogeneous catalysis and solid catalysts. *Ullmann's Encyclopedia of Industrial Chemistry*. United States: Wiley.

Lathiya, D.R., Bhatt, D.V. & Maheria, K.C. 2018. Synthesis of sulfonated carbon catalyst from waste orange peel for cost effective biodiesel production. *Bioresource Technology Reports* 2: 69-76.

Lee, D. 2013. Preparation of a sulfonated carbonaceous material from lignosulfonate and its usefulness as an esterification catalyst. *Molecules* 18(7): 8168-8180.

Liu, K., Wang, R. & Yu, M. 2018. An efficient, recoverable solid base catalyst of magnetic bamboo charcoal: Preparation, characterization, and performance in biodiesel production. *Renewable Energy* 127: 531-538.

Lokman, I.M., Rashid, U., Taufiq-Yap, Y.H. & Yunus, R. 2015. Methyl ester production from palm fatty acid distillate using sulfonated glucose-derived acid catalyst. *Renewable Energy* 81: 347-354.

Lokman, I.M., Rashid, U., Zainal, Z., Yunus, R. & Taufiq-Yap, Y.H. 2014. Microwave-assisted biodiesel production by esterification of palm fatty acid distillate. *Journal of Oleo Science* 63: 849-855.

Lotero, E., Liu, Y., Lopez, D.E., Suwannakarn, K., Bruce, D.A. & Goodwin, J.G. 2005. Synthesis of biodiesel via acid catalysis. *Industrial & Engineering Chemistry Research* 44(14): 5353-5363.

Malins, K., Brinks, J., Kampars, V. & Malina, I. 2016. Esterification of rapeseed oil fatty acids using a carbon-based heterogeneous acid catalyst derived from cellulose. *Applied Catalysis A: General* 519: 99-106.

Marinković, D.M., Stanković, M.V., Veličković, A.V., Avramović, J.M., Miladinović, M.R., Stamenković, O.O., Veljković, V.B. & Jovanović, D.M. 2016. Calcium oxide as a promising heterogeneous catalyst for biodiesel production: Current state and perspectives. *Renewable and Sustainable Energy Reviews* 56: 1387-1408.

Mengyu, G., Deng, P., Li, M., En, Y. & Jianbing, H. 2009. The kinetics of the esterification of free fatty acids in waste cooking oil using $Fe_2(SO_4)_3/C$ catalyst. *Chinese Journal of Chemical Engineering* 17(1): 83-87.

Nakatani, N., Takamori, H., Takeda, K. & Sakugawa, H. 2009. Transesterification of soybean oil using combusted oyster shell waste as a catalyst. *Bioresource Technology* 100(3): 1510-1513.

Nautiyal, P., Subramanian, K. & Dastidar, M. 2014. Kinetic and thermodynamic studies on biodiesel production from *Spirulina platensis* algae biomass using single stage extraction–transesterification process. *Fuel* 135: 228-234.

Okamura, M., Takagaki, A., Toda, M., Kondo, J.N., Domen, K., Tatsumi, T., Hara, M. & Hayashi, S. 2006. Acid-catalyzed reactions on flexible polycyclic aromatic carbon in amorphous carbon. *Chemistry of Materials* 18(13): 3039-3045.

Paul, A.K. 2018. Synthesis, structure and topological analysis of glycine templated highly stable cadmium sulfate framework: A new lewis acid catalyst. *Journal of Molecular Structure* 1157: 672-678.

Peng-Lim, B., Ganesan, S., Maniam, G.P. & Khairuddean, M. 2012. Sequential conversion of high free fatty acid oils into biodiesel using a new catalyst system. *Energy* 46(1): 132-139.

Ping, B.T.Y. & Yusof, M. 2009. Characteristics and properties of fatty acid distillates from palm oil. *Oil Palm Bulletin* 59: 5-11.

Rezaei, R., Mohadesi, M. & Moradi, G. 2013. Optimization of biodiesel production using waste mussel shell catalyst. *Fuel* 109: 534-541.

Sajab, M.S., Chia, C.H., Zakaria, S., Jani, S.M., Ayob, M.K., Chee, K.L., Khiew, P.S. & Chiu, W.S. 2011. Citric acid modified kenaf core fibres for removal of methylene blue from aqueous solution. *Bioresource Technology* 102(15): 7237-7243.

Sharma, Y., Singh, B. & Upadhyay, S. 2008. Advancements in development and characterization of biodiesel: A review. *Fuel* 87: 2355-2373.

Shuit, S.H. & Tan, S.H. 2014. Feasibility study of various sulphonation methods for transforming carbon nanotubes into catalysts for the esterification of palm fatty acid distillate. *Energy Conversion and Management* 88: 1283-1289.

Sirisomboonchai, S., Abuduwayiti, M., Guan, G., Samart, C., Abliz, S., Hao, X., Kusakabe, K. & Abudula, A. 2015. Biodiesel production from waste cooking oil using calcined scallop shell as catalyst. *Energy Conversion and Management* 95: 242-247.

Soriano Jr., N.U., Venditti, R. & Argyropoulos, D.S. 2009. Biodiesel synthesis via homogeneous lewis acid-catalyzed transesterification. *Fuel* 88(3): 560-565.

Su, F. & Guo, Y. 2014. Advancements in solid acid catalysts for biodiesel production. *Green Chemistry* 16(6): 2934-2957.

532

Sundar, S., Venkatachalam, G. & Kwon, S.J. 2018. Biosynthesis of copper oxide (CuO) nanowires and their use for the electrochemical sensing of dopamine. *Nanomaterials* 8(10): 823.

Supamathanon, N., Wittayakun, J. & Prayoonpokarach, S. 2011. Properties of Jatropha seed oil from northeastern Thailand and its transesterification catalyzed by potassium supported on NaY zeolite. *Journal of Industrial and Engineering Chemistry* 17(2): 182-185.

Suppalakpanya, K., Ratanawilai, S. & Tongurai, C. 2010. Production of ethyl ester from esterified crude palm oil by microwave with dry washing by bleaching earth. *Applied Energy* 87(7): 2356-2359.

Takeshita, T., Ohnishi, R. & Tanabe, K. 1974. Recent survey of catalysis by solid metal sulfates. *Catalysis Reviews* 8(1): 29-63.

Theivasanthi, T. & Alagar, M. 2010. X-ray diffraction studies of copper nanopowder. *arXiv preprint* arXiv:1003.6068.

Thushari, I. & Babel, S. 2018a. Preparation of solid acid catalysts from waste biomass and their application for microwave-assisted biodiesel production from waste palm oil. *Waste Management & Research* 36(8): 719-728.

Thushari, P. & Babel, S. 2018b. Biodiesel production from waste palm oil using palm empty fruit bunch-derived novel carbon acid catalyst. *Journal of Energy Resources Technology* 140(3): 032204.

Uzun, B.B., Kılıç, M., Özbay, N., Pütün, A.E. & Pütün, E. 2012. Biodiesel production from waste frying oils: Optimization of reaction parameters and determination of fuel properties. *Energy* 44(1): 347-351.

Watanabe, Y., Shimada, Y., Sugihara, A., Noda, H., Fukuda, H. & Tominaga, Y. 2000. Continuous production of biodiesel fuel from vegetable oil using immobilized *Candida antarctica* lipase. *Journal of the American Oil Chemists' Society* 77(4): 355-360.

Xia, P., Liu, F., Wang, C., Zuo, S. & Qi, C. 2012. Efficient mesoporous polymer based solid acid with superior catalytic activities towards transesterification to biodiesel. *Catalysis Communications* 26: 140-143.

Xue, W., Sun, L., Yang, F., Wang, Z. & Li, F. 2016. Peanut shell-derived carbon solid acid with large surface area and its application for the catalytic hydrolysis of cyclohexyl acetate. *Materials* 9(10): 833.

Yu, D., Tian, L., Wu, H., Wang, S., Wang, Y., Ma, D. & Fang, X. 2010. Ultrasonic irradiation with vibration for biodiesel production from soybean oil by Novozym 435. *Process Biochemistry* 45(4): 519-525.

Yujaroen, D., Goto, M., Sasaki, M. & Shotipruk, A. 2009. Esterification of palm fatty acid distillate (PFAD) in supercritical methanol: Effect of hydrolysis on reaction reactivity. *Fuel* 88(10): 2011-2016.

Zhang, J. & Jiang, L. 2008. Acid-catalyzed esterification of *Zanthoxylum bungeanum* seed oil with high free fatty acids for biodiesel production. *Bioresource Technology* 99(18): 8995-8998.

Zhu, S., Chen, M., Ren, W., Yang, J., Qu, S., Li, Z. & Diao, G. 2015. Microwave assisted synthesis of α-Fe_2O_3/reduced graphene oxide as anode material for high performance lithium ion batteries. *New Journal of Chemistry* 39(10): 7923-7931.

Zong, M.H., Duan, Z.Q., Lou, W.Y., Smith, T.J. & Wu, H. 2007. Preparation of a sugar catalyst and its use for highly efficient production of biodiesel. *Green Chemistry* 9(5): 434-437.

Rahila Ishfaq*, Nurun Najwa Ruslan, Suzi Salwah Jikan & Amira Saryati Ameruddin
Faculty of Applied Sciences and Technology
Universiti Tun Hussein Onn Malaysia
86400 Parit Raja, Johor Darul Takzim
Malaysia

Nursyafreena Attan
Faculty of Science
Universiti Teknologi Malaysia
81310 UTM, Johor Darul Takzim
Malaysia

*Corresponding author; email: rahilanaz.ishfaq@gmail.com